Experimental Verification of 6th Radial Force Control for IPMSMs Based on Flux Linkage

Masato Kanematsu
Hiroshi Fujimoto, and Yoichi Hori
The University of Tokyo
5-1-5 Kashiwanoha,
Kashiwa, Chiba, 277-8561 Japan
kanematsu@hflab.k.u-tokyo.ac.jp
fujimoto, hori@k.u-tokyo.ac.jp

Toshio Enomoto, Masahiko Kondou, Hiroshi Komiya
Kantaro Yoshimoto, and Takayuki Miyakawa
Nissan Motor Co., Ltd.
1-1, Morinosatoaoyama, Atsugi-shi
Kanagawa, 243-0123, Japan
enomoto, m-kondo, h-komiya@mail.nissan.co.jp
ka-yoshimoto, takayuki_miyakawa@mail.nissan.co.jp

***Abstract*—IPMSMs (Interior Permanent Magnet Synchronous Motors) are widely used for many industrial applications. However, IPMSMs cause large noise and vibration due to torque ripple and radial force. In this paper, 6th radial force caused by harmonic current is analyzed and modelling of 6th radial force is constructed based on flux linkage Based on this modelling, 6th radial force is mitigated by injecting harmonic currents. Firstly, we make some assumptions to make 6th radial force modelling. Secondly, 6th radial force modelling is derived. Simulation results and Experimental results verify the validity of 6th radial force model. Finally, 6th radial force control is performed by injecting dq-axis harmonic current.**

I. INTRODUCTION

In many industrial applications, IPMSMs (Interior Permanent Magnet Synchronous Motors) are often selected as drive motors. In these applications, IPMSMs face strong demands about the reduction of noise and vibration. Specially the noise and vibration problems in the inside of cars remain to be one of the problems which should be solved. Furthermore lower acoustic noise and vibration is desirable to enhance the value of products[1].

Techniques to minimize the acoustic noise and vibration are classified into three categories, analysis techniques, mechanical designing techniques, and current excitation techniques. The techniques to analyze and predict the acoustic noise and vibration caused by electromagnetic force are investigated in [2][3][4] and [5]. These researches focus on stator deformations and make comparisons between Finite Element Analysis(FEA) and experimental result. Generally, the noise and vibration can be reduced by mechanical designings and current excitation techniques. The Reference [6] proposes the structural designing to reduce radial force vibration. The considerations of Skewing methods [7][8][9] and pole slot combination[10] are also effective to reduce the vibration of radial force. However, the methods with structural designing usually increase the cost of the products and make it complicated to design motor topologies. Therefore we focus on the methods to reduce radial force with current excitation.

It is known that in IPMSMs electrical 2nd and 6th radial forces usually cause serious noise and vibration. There exist phase differences between the 2nd radial force on U, V and W-phase tooth as:

$$F_{rU}(\theta) = F_{r2}\cos 2\theta \quad (1)$$

$$F_{rV}(\theta) = F_{r2}\cos 2\left(\theta - \frac{2}{3}\pi\right) \quad (2)$$

$$F_{rW}(\theta) = F_{r2}\cos 2\left(\theta - \frac{4}{3}\pi\right) \quad (3)$$

where F_{r2} is the amplitude of 2nd radial force. These radial forces cause Pth order annular elastic deformation, where P denotes pole pairs. 2nd radial force modelling and control method have been proposed in [11]. Jiao *et al.* [12] also focuses on 2nd radial force reduction.

On the other hand, 6th radial forces on U, V and W-phase tooth are in phase as:

$$F_{rU}(\theta) = F_{r6}\cos 6\theta \quad (4)$$

$$F_{rV}(\theta) = F_{r6}\cos 6\left(\theta - \frac{2}{3}\pi\right) \quad (5)$$

$$F_{rW}(\theta) = F_{r6}\cos 6\left(\theta - \frac{4}{3}\pi\right) \quad (6)$$

Therefore the transfer characteristics from radial force to acceleration has very high amplitude because 6th radial force excites spatially 0th annular mode and it is a critical issue to suppress 6th radial force. W. Zhu *et al.* [13] proposes current excitation method to suppress harmonic radial force with harmonic current. However, this method needs iterative calculations of electromagnetic field analysis at one drive condition and it is not practical to reduce motor vibration with this theory at any drive conditions. Therefore, simpler and more intuitive modelling which can be installed in current controllers are desired. Fig. 1 shows the concept of 2nd and 6th radial force and typical natural frequency mode of the stator.

Generally, to control harmonic radial forces by current excitation the relationship between current and radial force should be formulated. Z.Q. Zhu [14] proposes the analytical formulation of radial force distibution caused by current and magnet flux by expanding the flux distribution as a Fourier series. However, this method is hard to install current controller

978–1–4799–5776–7/14/$31.00

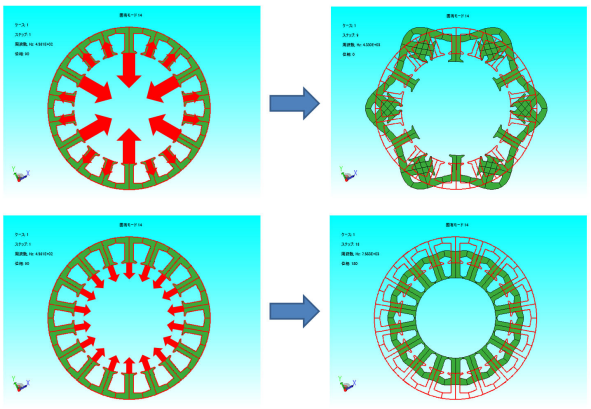

Fig. 1. Typical natural frequency mode of stator(12P18S)

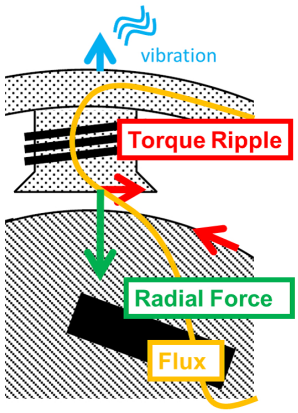

Fig. 2. The magnetic attractive force in IPMSMs

because of the complexity. In this paper, 6th component of the radial force on a tooth is expressed simply based on flux linkage. This expression clarifies the relationship between dq-axis harmonic current and 6th radial force and enables us to control 6th radial force. Fig. 3 shows the subject of our research. The simulation and experiment are performed to validate the utility of the modelling and suppression control method.

II. Assumption of Approximation

In this chapter, the assumptions of approximations are shown. Based on these assumptions, approximation model of 6th radial force is derived. JMAG (electromagnetic field analysis software) produced by JSOL Corporation is utilized for this analysis.

A. The relationship between current, flux linkage and radial force

Flux linkage through a U-phase tooth $\phi_u(t)$ is expressed as

$$\phi_u(t) = \frac{\psi_u(t)}{N} \tag{7}$$

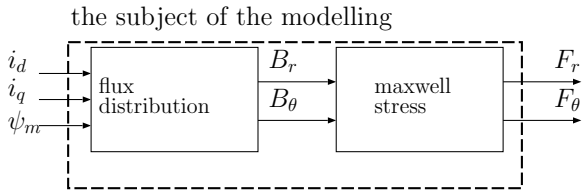

Fig. 3. The relationship between current to radial force

where, N is turn number per a phase and ψ_u is flux linkage on U-phase tooth.

We assume the tangential flux distribution $B_\theta(t)$ is small, and all flux linkage is generated by the radial flux distribution $B_r(t)$.

$$\phi_u(t) = \int B_r(t) dS \tag{8}$$

Radial force on a U-phase tooth $f_u(t)$ is calculated based on Maxwell stress.

$$f_u(t) = \int \frac{B_r(t)^2}{2\mu_0} dS \tag{9}$$

where S is a tooth area facing air region. This paper has the assumption that flux is distributed equally over the tooth area S. With this assumption, (8) and (9) are rewritten as (10) and (11).

$$\phi_u(t) = B_r(t) S \tag{10}$$

$$f_u(t) = \frac{B_r^2(t)}{2\mu_0} S \tag{11}$$

In this paper, we consider constant speed condition and radial force is regarded as a function for electrical angle θ. Substituting (7) and (10) into (11), equation (12) is obtained.

$$f_u(\theta) = \frac{\psi_u^2(\theta)}{2\mu_0 S N^2} = A\psi_u^2(\theta) \tag{12}$$

$$A := \frac{1}{2\mu_0 S N^2} \tag{13}$$

(12) is called the approximation of radial force in this paper.

B. Assumption on flux linkage

It is also assumed that flux linkage caused by permanent magnet $\psi_{um}(\theta)$ and flux linkage caused by current $\psi_{ui}(\theta)$ satisfy linear independency.

$$\psi_u(\theta) = \psi_{um}(\theta) + \psi_{ui}(\theta) \tag{14}$$

This paper considers 12 poles 18 slots IPMSM. The winding pattern is concentrated winding. To consider 6th radial force, $\psi_{um}(\theta)$ is defined as:

$$\psi_{um}(\theta) = \psi_{1m}\cos\theta + \psi_{5m}\cos 5\theta + \psi_{7m}\cos 7\theta \tag{15}$$

5th and 7th flux linkage ψ_{5m} and ψ_{7m} have negative value when they have opposite phase against fundamental flux linkage. On ground of the symmetry, flux linkage on U-phase tooth

TABLE I. PARAMETERS OF IPMSM

turn number N	120
a pair of poles P	6
teeth area S [m^2]	4.13×10^{-4}
ψ_{m1}[mWb]	36.2
ψ_{m5}[mWb]	0.811
ψ_{m7}[mWb]	-0.114
L_d[mH]	0.866
L_q[mH]	1.31

is considered. The parameter of IPMSM is shown in Table II. dq-axis current reference i_d, i_q is defined as :

$$\begin{aligned} i_d &:= I_{d0} + i_{d6} && (16)\\ i_{d6} &:= I_{d6}\cos(6\theta - \theta_{d6}) && (17)\\ i_q &:= I_{q0} + i_{q6} && (18)\\ i_{q6} &:= I_{q6}\cos(6\theta - \theta_{q6}) && (19) \end{aligned}$$

III. THE INFLUENCE OF d-AXIS HARMONIC CURRENT

Flux linkage on U-phase caused by d-axis harmonic current ψ_{uih} is shown as:

$$\begin{bmatrix}\psi_{uih}\\ \psi_{vih}\\ \psi_{wih}\end{bmatrix} = \boldsymbol{C}_{dq}^{uvw}\begin{bmatrix}L_d I_{d6}\cos(6\theta - \theta_{d6})\\ 0\end{bmatrix}$$

$$= \sqrt{\frac{1}{6}}L_d I_{d6}\begin{bmatrix}\cos(5\theta - \theta_{d6}) + \cos(7\theta - \theta_{d6})\\ \cos(5\theta - \theta_{d6} + \frac{2}{3}\pi) + \cos(7\theta - \theta_{d6} - \frac{2}{3}\pi)\\ \cos(5\theta - \theta_{d6} + \frac{4}{3}\pi) + \cos(7\theta - \theta_{d6} - \frac{4}{3}\pi)\end{bmatrix} \quad (20)$$

Adding harmonic flux linkage ψ_{uih}, all flux linkage on U-phase is written by :

$$\begin{aligned}\psi_u(\theta) =& \sqrt{\frac{2}{3}}(\Psi_{1m} + L_d I_{d0})\cos\theta - \sqrt{\frac{2}{3}}L_q I_{q0}\sin\theta\\ &+ \psi_{5m}\cos 5\theta + \sqrt{\frac{1}{6}}L_d I_{d6}\cos(5\theta - \theta_{d6})\\ &+ \psi_{7m}\cos 7\theta + \sqrt{\frac{1}{6}}L_d I_{d6}\cos(7\theta - \theta_{d6}) \quad (21)\end{aligned}$$

where, $\Psi_{1m} := \sqrt{\frac{3}{2}}\psi_{1m}$. In this paper, 2-phase/3-phase transform is absolute transformation. Substituting (21) into (12), the 6th order component generated by d-axis harmonic current is extracted as :

$$\begin{aligned} f_{i_{d6}}(I_{d0}, I_{q0}, I_{d6}, \theta_{d6}) &= \frac{A}{3}(\Psi_{1m} + L_d I_{d0})L_d I_{d6}\cos(6\theta - \theta_{d6})\\ &= K_{dr}(I_{d0}, I_{q0})i_{d6} \quad (22)\end{aligned}$$

$$K_{dr}(I_{d0}, I_{q0}) := \frac{A}{3}(\Psi_{1m} + L_d I_{d0})L_d \quad (23)$$

where $f_{i_{d6}}(I_{d0}, I_{q0}, I_{d6}, \theta_{d6})$ is 6th radial force caused by i_{d6}. To verify the accuracy of (22), FEA is performed on the condition that $I_{d6} = 1$A and $\theta_{d6} = 0$deg. The FEA result is shown in Fig.4. Although a lot of assumptions have been made to lead (22), we can see that 6th radial force model (22) differs very little from FEA result.

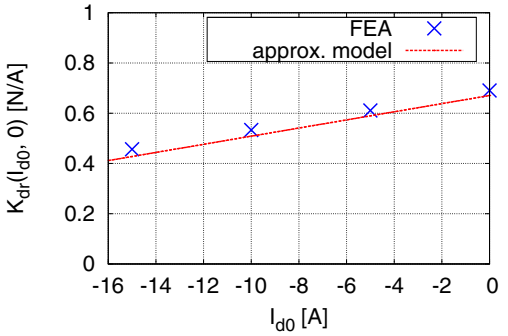

(a) $K_{dr}(I_{d0}, 0)$ when I_{d0} varies

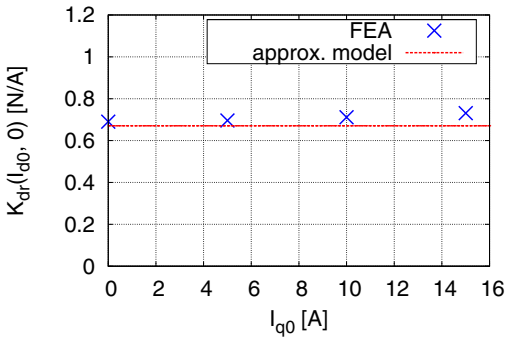

(b) $K_{dr}(0, I_{q0})$ when I_{q0} varies

Fig. 4. The comparison between $K_{dr}(I_{d0}, I_{q0})$ and FEA results

IV. THE INFLUENCE OF q-AXIS HARMONIC CURRENT

In the same way, flux linkage generated by q-axis harmonic current $\psi_{uih}(\theta)$ is calculated as:

$$\begin{bmatrix}\psi_{uih}(\theta)\\ \psi_{vih}(\theta)\\ \psi_{wih}(\theta)\end{bmatrix} = \boldsymbol{C}_{dq}^{uvw}\begin{bmatrix}0\\ L_q I_{q6}\cos(6\theta - \theta_{q6})\end{bmatrix}$$

$$= \sqrt{\frac{1}{6}}L_q I_{q6}\begin{bmatrix}\sin(5\theta - \theta_{q6}) - \sin(7\theta - \theta_{q6})\\ \sin(5\theta - \theta_{q6} + \frac{2}{3}\pi) - \sin(7\theta - \theta_{q6} - \frac{2}{3}\pi)\\ \sin(5\theta - \theta_{q6} + \frac{4}{3}\pi) - \sin(7\theta - \theta_{q6} - \frac{4}{3}\pi)\end{bmatrix} \quad (24)$$

Substituting (24) into (12), the 6th order component generated by q-axis harmonic current is extracted as:

$$\begin{aligned} f_{i_{q6}}(I_{d0}, I_{q0}) &= \frac{A}{3}L_q I_{q0}L_q I_{q6}\cos(6\theta - \theta_{q6}) \quad (25)\\ &= K_{qr}(I_{d0}, I_{q0})i_{q6} \quad (26)\end{aligned}$$

$$K_{qr}(I_{d0}, I_{q0}) := \frac{A}{3}L_q^2 I_{q0} \quad (27)$$

Fig.5 shows the FEA results which are performed on the condition that $I_{q6} = 1$A, $\theta_{q6} = 0$A, and $I_{d0} = 0$A. Fig.5 shows that Eq. (27) can predict 6th radial force caused by q-axis harmonic current well.

Next, to examine the effectiveness to apply motors which have different pole slot combinations, some FEA analyses are performed. Table II shows the motor parameters which are

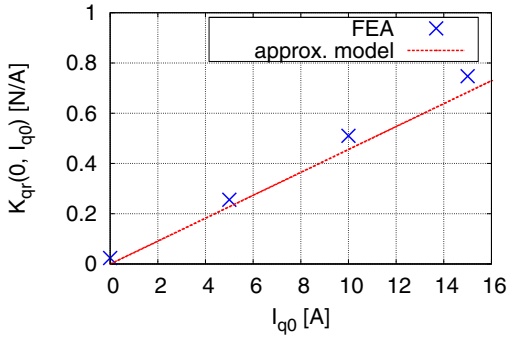

Fig. 5. $K_{qr}(0, I_{q0})$ when I_{q0} varies

TABLE II. PARAMETERS OF IPMSMS FOR COMPARATIVE VERIFICATION

motor type	8P12S	12P18S	16P24S
turn number N	120	120	120
a pair of poles P	4	6	8
teeth area S [mm^2]	621	413	325
ψ_{m1}[mWb]	63.0	36.2	22.8
L_d[mH]	1.04	0.866	0.621
L_q[mH]	1.85	1.31	0.817
airgap length	1mm		
stator outer diameter	150mm		
rotor outer diameter	100mm		
stack length	30mm		

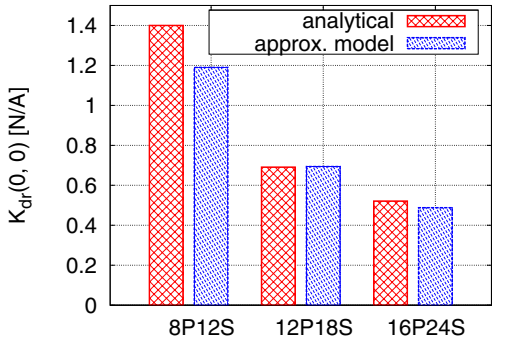

Fig. 6. FEA results of $K_{dr}(I_{d0}, I_{q0})$(comparison between different motors)

used in these comparative verification.

The accuracies of the approximation model $K_{dr}(I_{d0}, I_{q0})$ are validated in Fig. 6. In these three topologies, Approximate models correspond to FEA results pretty much. We can also see that small pole pairs lead to the deterioration of the accuracy of the approximation model. This is because spatial harmonics are effected largely in the motors of small pole pairs.

V. METHOD OF 6TH RADIAL FORCE CONTROL

The transfer characteristics between 6th harmonic current and 6th radial force have been obtained. All 6th radial force

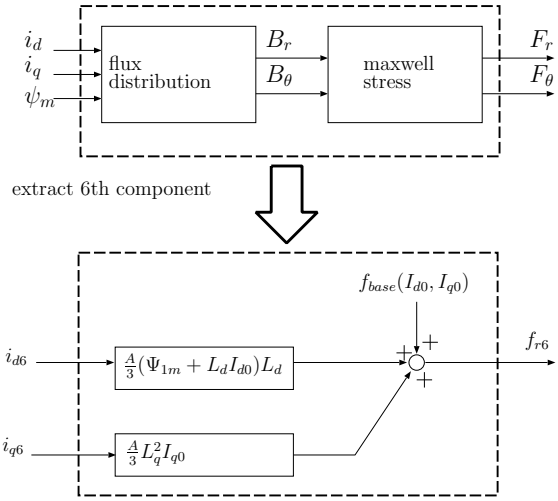

Fig. 7. block diagram of all 6th radial force

is expressed as

$$f_{r6}(i_d, i_q) = f_{\text{base}}(I_{d0}, I_{q0}) + K_{dr}(I_{d0}, I_{q0})i_{d6} + K_{qr}(I_{d0}, I_{q0})i_{q6} \quad (28)$$

$$f_{\text{base}}(I_{d0}, I_{q0}) := F_{\text{base}} \cos(6\theta - \theta_{\text{base}}) \quad (29)$$

where $f_{\text{base}}(I_{d0}, I_{q0})$ is 6th radial force caused by harmonic inductance and harmonic magnetic flux. The relationship of 6th radial force in Fig. 3 can be clarified as Fig. 7. 6th radial force control consists of 3 steps.

STEP 1:

First, $f_{\text{base}}(I_{d0}, I_{q0})$ needs to be obtained. This can be calculated by FEA on the condition that i_d and i_q are ideal sinusoidal currents.

STEP 2:

Second, $K_{dr}(I_{d0}, I_{q0})$ and $K_{qr}(I_{d0}, I_{q0})$ are calculated by Eq. (23) and (27).

STEP 3:

After that, an optimal harmonic current reference to suppress $f_{\text{base}}(I_{d0}, I_{q0})$ is obtained. Generally, i_{d6} is preferred to suppress $f_{\text{base}}(I_{d0}, I_{q0})$ because i_{d6} causes little deterioration of torque ripple compared with i_{q6}. The optimal harmonic current reference $i_{d6:\text{opt}}$ is decided as

$$i_{d6:\text{opt}} = -\frac{F_{\text{base}}(I_{d0}, I_{q0})}{K_{dr}(I_{d0}, I_{q0})} \cos(6\theta - \theta_{\text{base}}(I_{d0}, I_{q0})) \quad (30)$$

. Fig. 8 shows simulation result of 6th radial force control by d-axis harmonic current. 4th and 8th radial forces are affected by 6th d-axis current because 5th and 7th harmonic fluxes generated by 5th and 7th harmonic current produce 4th and 8th radial forces. However, considering transfer characteristics

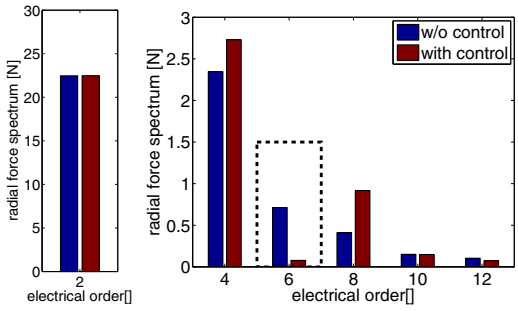

(a) 2nd (b) 4-12th order

Fig. 8. 6th radial force control by d-axis harmonic current(simulation result)

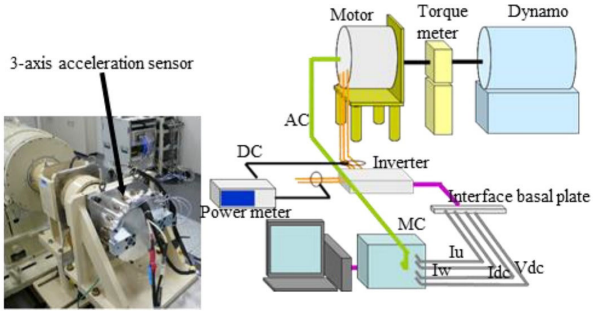

Fig. 9. Experimental Setup

of 4th and 8th radial forces, which has Pth annular mode, it is said that 4th and 8th radial forces cause little noise and vibration.

VI. Experimental Results

Experimental verifications are performed to show the validity of this control scheme. Fundamental experiments have been conducted in [15]. In this paper, test motor which has large capacity is used. Test motor and can be seen in Fig. 9. Dynamo controls the speed of the motor at 1000rpm. Harmonic currents are actively injected to test motor and the radial accelerations are measured by accelerometers. The current controller is designed as Perfect Tracking Control and Pole zero cancellation PI Control[16]. 6th radial acceleration $a_{r6}(\omega)$ is expressed theoretically as

$$a_{r6}(\omega) = H(\omega) f_{r6}(i_d, i_q). \tag{31}$$

where $H(\omega)$ is transfer characteristics between radial force and vibratoin at the speed of ω.

A. the accuracy of 6th radial force control

The experiment is performed on the condition that $I_{q0} = 50$ A, T=12.5 Nm. The harmonic current reference is calculated from Eq. (30) as:

$$I_{d6} = 10.1[\mathrm{A}] \tag{32}$$

$$\theta_{d6} = 205.8[\mathrm{deg}]. \tag{33}$$

To validate the optimal harmonic current phase, 6th radial accelerations are measured with shifting harmonic current

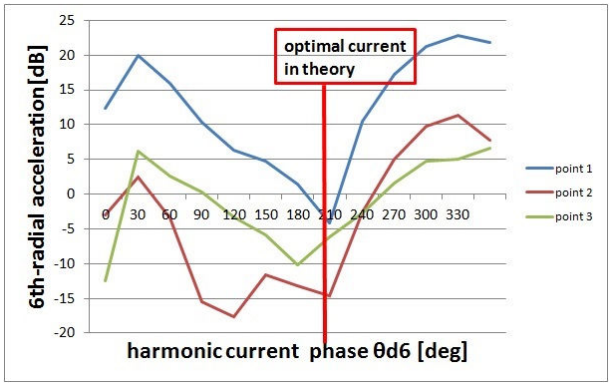

(a) the validation of 6th radial force control(phase)

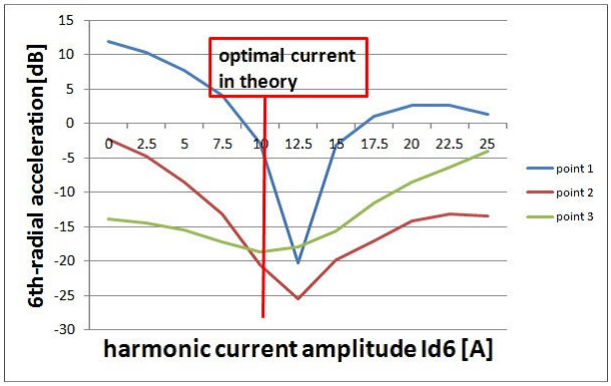

(b) the validation of 6th radial force control(amplitude)

Fig. 10. The validation of 6th radial force control(Experimental result)

phase. The amplitude of harmonic current I_{d6} is 20 A. Experimental results are shown in Fig. 10(b). 6th radial accelerations are largely decreased at the optimal phase. The accuracy of the optimal harmonic current amplitude is also validated in Fig. 10(a). It can be seen that 6th radial accelerations are mitigated by about 10dB. Furthermore, it is possible to realize more vibration reduction at $I_{q6} = 12.5$ A. This difference is considered to arise from the model error between FEA model and experimental setup and the modelling error proposed in this paper.

VII. Conclusion

In this paper, 6th radial force caused by harmonic current are formulated as Eq. (22) and (26). These formulations are simple and instuitive enough to apply current excitation. Based on these modellings, 6th radial force control is proposed. d-axis 6th harmonic current is injected actively and 6th radial force is largely suppressed. The effectiveness of this control method is verified by FE Analyses and experiments.

In previous researches, the relationship between the desinging methods to reduce motor vibration and the current excitation to suppress motor vibration is not clear. The radial force modelling proposed in this paper is expressed by motor parameter. This research helps to realize combination schemes of current excitation and motor designing.

REFERENCES

[1] Kondo Keiichiro, Kubota Hisao: "Innovative Application Technologies of AC Motor Drive Systems", IEEJ Trans. Industry Applications, Vol.1, No.3 pp.132-140, 2012

[2] M.Islam, R.Islam, T.Sebastian : "Noise and vibration characteristics of permanent magnet synchronous motors using electromagnetic and structural analyses", IEEE International Conference on Energy Conversion Congress and Exposition (ECCE), Vol.17, No.22, pp.3399-3405,2011

[3] H.Y.Issac Du, Lei Hao, and Hejie Lin: "Modeling and analysis of electromagnetic vibrations in fractional slot PM machines for electric propulsion," Energy Conversion Congress and Exposition (ECCE), pp.5077-5084(2013)

[4] J.F. Gieras, Chong Wang, Joseph. C.S.Lai, Nesimi Ertugrul: "Analytical Prediction of Noise of Magnetic Origin Produced by Permanent Magnet Brushless Motors," IEEE International Conference on Electric Machines Drives Conference(IEMDC), Vol.1, No.5, pp.148-152(2007)

[5] M. Boesing, R.W. De Doncker: "Exploring a Vibration Synthesis Process for the Acoustic Characterization of Electric Drives" IEEE Trans. Ind. Appl., vol.48, no.1, pp.70-78(2012)

[6] Sang-Ho Lee, Jung-Pyo Hong, Sang-Moon Hwang, Woo-Taik Lee, Ji-Young Lee, Young-Kyoun Kim: "Optimal Design for Noise Reduction in Interior Permanent-Magnet Motor", IEEE Trans. Ind. Appl., vol.45, no.6, pp.1954-1960, Nov.-dec. 2009

[7] D. C. Hanselman: "Effect of skew, pole count and slot count on brushless motor radial force, cogging torque and back EMF", Inst. Elect. Eng. Proc. mdash,Elect. Power Appl., Vol.144, No.5, pp.325-330, 1997

[8] Jae-Woo Jung, Do-Jin Kim, Jung-Pyo Hong, Geun-Ho Lee, Seong-Min Jeon: "Experimental Verification and Effects of Step Skewed Rotor Type IPMSM on Vibration and Noise", IEEE Trans. Magn., vol.47, no.10, pp.3661-3664, 2011

[9] A. Cassat, C. Espanet, R. Coleman, L. Burdet, E. Leleu,D. Torregrossa, J. M' Boua, A. Miraoui: "A Practical Solution to Mitigate Vibrations in Industrial PM Motors Having Concentric Windings", IEEE Trans. Ind. Appl., vol.48, no.5, pp.1526-1538, 2012

[10] M.Valavi, A.Nysveen, R.Nilssen, R.D.Lorenz, T. Rolvag: "Influence of Pole and Slot Combinations on Magnetic Forces and Vibration in Low-Speed PM Wind Generators", IEEE Trans. Magn., vol.50, no.5, pp.1-11, May 2014

[11] M.Kanematsu, T.Miyajima, H.Fujimoto, Y.Hori, T.Enomoto, M.Kondou, H.Komiya, K.Yoshimoto, T.Miyakawa: "Suppression Control of Radial Force Vibration due to Fundamental Permanent-Magnet Flux in IPMSM", IEEE Energy Conversion Congress and Exposition(ECCE), pp.2812-2816, 2013

[12] Jiao Guandong, C.D.Rahn : "Field weakening for radial force reduction in brushless permanent-magnet DC motors", IEEE Trans. Magnetics, Vol.40, No.5, pp. 3286- 3292, 2004

[13] W. Zhu, B. Fahimi, and S. Pekarek: "A field reconstruction method for optimal excitation of surface mounted permanent magnet synchronous machines", IEEE Trans. Ene. Conv., vol. 21, no. 2, pp. 303-313, Jun. 2006

[14] Z.Q. Zhu, Z. Xia, L. Wu, and G. Jewell: "Analytical modeling and Finite-element computation of radial vibration force in fractional-slot permanent-magnet brushless machines", IEEE Trans. Ind. Appl., vol. 46, no. 5, pp. 1908-1918, Sep./Oct. 2010

[15] M. Kanematsu, et al.: "Proposal of 6th Radial Force Control Based on Flux Linkage", The 2014 IEEE International Power Electronics Conference-ECCE ASIA-(IPEC), pp.2421-2426, May 2014

[16] K.Nakamura, H.Fujimoto, M.Fujitsuna: "Torque ripple suppression control for PM motor with current control based on PTC", 2010 International Power Electronics Conference (IPEC), pp.1077-1082, June 2010